



# Spatial pattern regression for meteorological fields interpolation

Vihotogbé Houssou<sup>1,2</sup> and Julie Carreau<sup>1,2,3,4</sup>

<sup>1</sup>Department of Mathematics and Industrial Engineering, Polytechnique Montréal, 2500 chemin de Polytechnique, Montréal, H3T 1J4, Québec, Canada

<sup>2</sup>GERAD - Groupe d'Études et de Recherche en Analyse des Décisions, 2920 Chemin de la Tour, Montréal, H3T 1N8, Québec, Canada

<sup>3</sup>Mila - Quebec Artificial Intelligence Institute, 6666 Saint-Urbain, Montréal, H2S 3H1, Québec, Canada

<sup>4</sup>IVADO - Institute for Data Valorization, 950 Av. Beaumont, Montréal, H3N 1V5, Québec, Canada

**Correspondence:** Vihotogbé Houssou (vihotogbe-2.houssou@polymtl.ca)

**Abstract.** High-resolution gridded meteorological data are essential for hydrological impact studies, yet their reconstruction from sparse station networks remains challenging. We introduce Spatial Pattern Regression (SPR), a data-driven method that reconstructs gridded meteorological fields by combining spatial information extracted from high-resolution regional climate model (RCM) simulations with station observations. SPR operates in two steps: spatial patterns are first extracted from RCM data using principal component analysis, then daily fields are reconstructed through linear regression using available observations. The method is first evaluated using controlled synthetic experiments, where virtual stations selected as a subset of the RCM grid emulate observational networks with varying density, size, and location. SPR is then validated using real station observations. Daily precipitation, minimum temperature, and maximum temperature are considered. Results show that SPR performs better than inverse distance weighting, ordinary kriging, and kriging with external drift, particularly under sparse network conditions. Sensitivity analyses highlight the dominant role of station density and location on interpolation accuracy, supporting the robustness and applicability of SPR for hydrological studies.

## 1 Introduction

High-resolution gridded meteorological data play a central role in hydrological impact studies, particularly in the context of climate change, where the frequency and intensity of extreme events such as heatwaves, heavy precipitation, and flooding are increasing (Warren et al., 2022). Hydrological models used for flood forecasting, water resource management, or climate impact assessments require meteorological inputs that accurately represent both spatial heterogeneity and extremes at fine spatial and temporal resolution. For example, Lucas-Picher et al. (2020) successfully reproduced the extreme flooding of the Richelieu River (southern Quebec, Canada) in spring 2011 using a high-resolution gridded hydrometeorological dataset at approximately 7 km resolution, which accounted for orographic precipitation effects (Livneh et al., 2015). Similarly, high-resolution meteorological fields have been shown to be critical for assessing heat-related impacts in urban environments (Lauer et al., 2023).

In practice, gridded meteorological data used in hydrological studies are typically obtained through three main approaches: spatial interpolation of station observations, physics-based numerical models (including numerical weather prediction and



regional climate models), and reanalysis products (Leduc et al., 2019; Gasset et al., 2021). Physics-based models, such as  
25 numerical weather prediction and regional climate models (RCMs), provide spatially complete and physically consistent meteorological fields at increasingly fine resolutions. These datasets are widely used in hydrological impact studies, either directly or after bias correction (e.g., Faghih and Brissette, 2023). However, raw model outputs may exhibit systematic biases and do not necessarily reproduce observed weather conditions at specific locations or times.

Spatial interpolation methods rely on statistical techniques to estimate meteorological variables at ungauged locations based  
30 on nearby observations. While widely used, their performance is strongly sensitive to station density and spatial variability, which are often limited, particularly in mountainous or sparsely instrumented regions (Ly et al., 2013). Under such conditions, spatial interpolation methods often struggle to capture realistic spatial variability, which can propagate errors into hydrological simulations (Hwang et al., 2012). This limitation becomes particularly critical during extreme rainfall events, where forecast accuracy strongly depends on network density (Segond et al., 2007; Looper and Vieux, 2012). To mitigate these limitations,  
35 auxiliary gridded information such as topography or climatology is commonly incorporated (Livneh et al., 2015; Werner et al., 2019). However, the use of climatology, often derived from RCM, is a limited way of exploiting the rich spatial structure present in RCM simulations.

The main contribution of this paper is the development of an interpolation method that exploits the spatial structure of RCM simulations through spatial patterns, which succinctly summarize the spatial structures present in these simulations.  
40 Specifically, we introduce Spatial Pattern Regression (SPR), a data-driven method that can be viewed as an intermediate between spatial interpolation and reanalysis. SPR assumes that high-resolution regional climate model simulations adequately represent the dominant spatial structures of meteorological variables. These spatial structures are first extracted from RCM data using principal component analysis (PCA), yielding spatial patterns that represent the principal modes of spatial organization of the variable. When handling the high dimensionality of gridded climate data, PCA (equivalent to Empirical Orthogonal  
45 Function - EOF) provides a well-established framework for identifying a limited number of dominant spatial patterns that explain most of the variability and that can be exploited in regression-type reconstructions (Monahan et al., 2009). Daily meteorological fields are then reconstructed through linear regression using observations from available stations, allowing spatial coherence to be imposed even under sparse network conditions. The use of dominant modes of variability extracted from covariance structures has been explored as a means to reconstruct spatially continuous fields when observations are  
50 sparse (Taylor et al., 2013).

SPR is evaluated against commonly used baseline interpolation methods. Performance is assessed using controlled synthetic experiments which enable systematic evaluations that would not be feasible using observations alone. In addition to these controlled synthetic experiments, an evaluation using real station observations is performed, thereby assessing both methodological robustness and practical applicability. Daily precipitation, minimum temperature, and maximum temperature are considered,  
55 as these variables are central to hydrological modeling and climate impact studies.

The remainder of this paper is organized as follows. Section 2 presents the study area and the datasets used, including regional climate model simulations and station observations. Section 3 describes the proposed Spatial Pattern Regression (SPR) methodology, the baseline interpolation methods, and the experimental design. Section 4 presents the results obtained from both



synthetic experiments and the independent validation using real observations. Finally, section 5 discusses the implications of the results for hydrological applications, as well as the limitations of the proposed approach. It also summarizes the main findings and outlines perspectives for future work.

## 2 Study area and Data

To evaluate and compare the interpolation methods, we considered daily precipitation ( $mm\ day^{-1}$ ) and minimum and maximum temperature ( $^{\circ}C$ ). These meteorological variables are commonly used as inputs in hydrological modeling and climate impact studies.

### 2.1 Regional climate model data

High-resolution gridded meteorological data were obtained from the ClimEx project, which investigates the impacts of climate change on extreme meteorological and hydrological events using the Canadian RCM (Leduc et al., 2019). The ClimEx simulations cover a North American domain discretized on a regular grid of  $280 \times 280$  cells, with a horizontal resolution of approximately 11 km (see Fig. 1a).

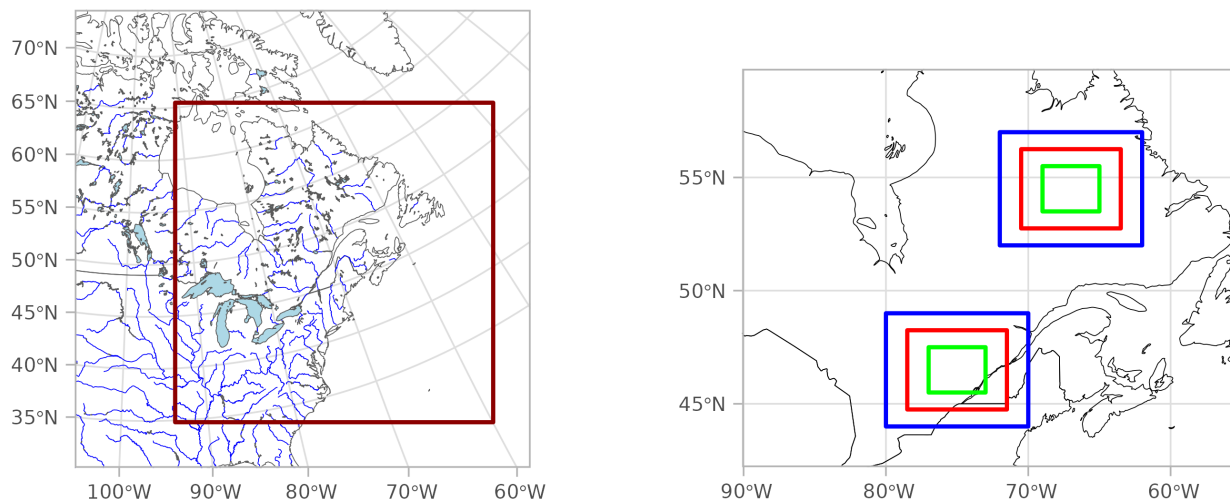
From the full ClimEx simulation period (1950–2099), two distinct periods were defined. An auxiliary period (1980–2009) was used to extract spatial information, including climatologies and spatial patterns. An interpolation period (2000–2009) was used to perform spatial reconstructions and to evaluate method performance (see § 3.4.1). Although the auxiliary and interpolation periods overlap in this study, the proposed methodology does not require temporal overlap or synchronicity between these periods, allowing flexibility in practical applications.

Within the North American ClimEx domain, two study regions were defined: a southern region and a northern region, reflecting contrasting climatic and spatial variability conditions. For each region, three nested spatial extents (large, medium, and small) were considered to assess the sensitivity of interpolation performance to region size (see Fig. 1b).

### 2.2 Observational data

Instrumented meteorological observations were obtained from the official monitoring network operated by Environment and Climate Change Canada (ECCC), which provides long-term, quality-controlled climate observations ([https://climate.weather.gc.ca/climate\\_data/bulk\\_data\\_e.html](https://climate.weather.gc.ca/climate_data/bulk_data_e.html), accessed January 30, 2026). The analysis is restricted to stations located in southern Quebec, within a spatial domain of approximately  $70\ 000\ km^2$ , defined by latitudes  $45.0\text{--}47.0^{\circ}N$  and longitudes  $75.0\text{--}70.0^{\circ}W$ .

Stations were selected to ensure strictly continuous observation periods, with no missing daily values and no gap filling. For each variable, a two-year period with 100% data completeness was retained in order to balance temporal representativeness and station availability. Different periods were selected across variables to maximize the number of available complete stations (Precipitation: October 8, 2000 – October 7, 2002 ; Minimum temperature: December 7, 2000 – December 6, 2002 ; Maximum temperature: December 12, 2016 – December 11, 2018).



(a) North American domain of the ClimEx project (dark red rectangle).

(b) Two study regions—referred to as the south and north regions—within the domain outlined in dark red in Fig. 1a, shown at three different sizes (in different colours).

**Figure 1.** Spatial domains used in this study.

The final dataset consists of 15 stations for precipitation and 44 stations for minimum and maximum temperature, each providing complete daily records over the corresponding two-year period. These observations are used exclusively for independent validation and do not contribute to the extraction of spatial patterns, ensuring a strict separation between auxiliary model information and real-world observations.

### 3 Methods

#### 3.1 From Climatology to Spatial Patterns

Climatologies, often used as auxiliary information in interpolation methods, are broadly defined as inter-annual averages of a given meteorological variable. When applied to RCM gridded data, this averaging process reveals little about the underlying spatial structure inherent to RCM simulations. In this study, we extract richer information from RCM simulations by characterizing their spatial patterns — a concept related to weather types or regimes frequently used in climate science, identified through clustering in empirical orthogonal function (EOF) space (Cattiaux et al., 2010).

More specifically, we define a spatial pattern as a spatially coherent structure that captures a recurrent mode of variability of a meteorological field over a given region. Such patterns describe how values tend to co-vary in space, independently of their instantaneous amplitude. Unlike climatologies, which represent long-term mean states, spatial patterns retain detailed



information on spatial variability. Furthermore, unlike local interpolation weights or distance-based kernels, they provide a global representation of spatial organization that remains meaningful even in areas with no direct observations.

105 Spatial patterns play a central role in the proposed SPR method by serving as a low-dimensional basis onto which daily meteorological data can be projected. Indeed, in practice, we compute the spatial patterns as the EOFs obtained through principal component analysis (PCA) of gridded RCM simulations. Each pattern corresponds to an eigenvector of the spatial covariance structure and represents an orthogonal mode of variability ordered by explained variance. Importantly, these patterns are extracted independently of the station observations used for reconstruction, ensuring that the spatial structures are not  
110 conditioned by the observational network geometry.

Unlike external covariates or drift terms used in some interpolation methods, spatial patterns encode intrinsic spatial variability derived directly from the meteorological field itself (Monahan et al., 2009; Carreau and Guinot, 2021). Their relevance depends on the variable and regional context, with complex fields such as precipitation typically requiring more patterns than temperature. As such, spatial patterns do not act as predictors of local magnitude but as structural building blocks that constrain  
115 the shape of the reconstructed field.

The extracted spatial patterns (see Fig. 2) are illustrated in the following to highlight their physical interpretability and role in the reconstruction framework.

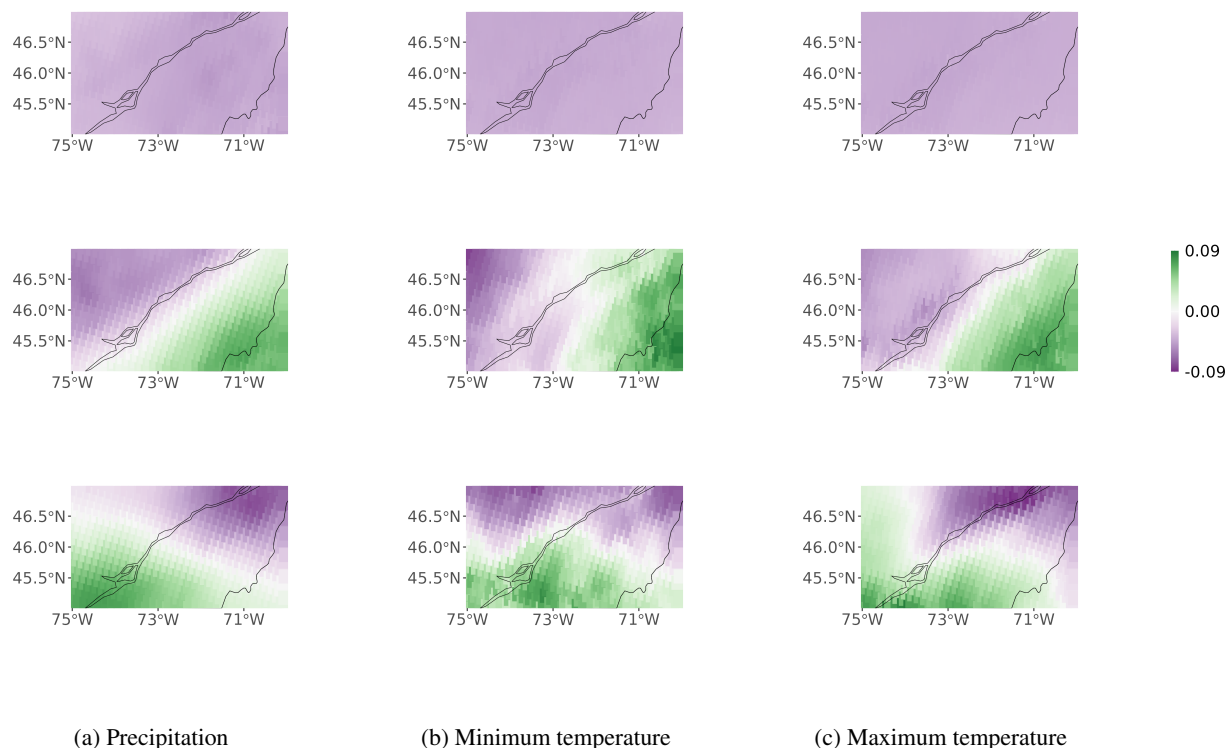


**Figure 2.** First three spatial patterns for each variable in the southern region (577 grid cells; see Fig. 1b), ordered from top to bottom by decreasing explained variance. Spatial patterns are dimensionless.

### 3.2 Spatial Pattern Regression (SPR)

SPR is the main methodological contribution of this paper: as its name indicates, it is based on the projection — performed via linear regression — of sparse station observations onto spatial patterns derived from RCM simulations. As SPR reconstructs spatially continuous meteorological fields from such observations, it can be regarded as an interpolation method, although its underlying mechanisms differ fundamentally from those of classical spatial interpolation approaches. It makes no distributional or stationarity assumptions and relies solely on the representativeness of the dominant spatial patterns. SPR consists of two main steps, each described in turn below.

#### 3.2.1 Identification of a representative basis of spatial patterns

The first step of SPR consists in extracting a representative basis of spatial patterns from high-resolution RCM simulations. These patterns are identified using Principal Component Analysis (PCA), computed via Singular Value Decomposition (SVD).



PCA provides an efficient way to extract a reduced set of orthogonal spatial modes that capture the dominant spatial variability of gridded meteorological fields (Link et al., 2019).

130 Let  $\mathbf{Z}_{n,p}^{\text{grid}}$  denote the RCM dataset over the auxiliary period, where  $n$  is the number of daily time steps and  $p$  is the number of grid cells in the study region. Applying SVD to the centered data matrix yields

$$\mathbf{Z}_{n,p}^{\text{grid}} = \mathbf{U}_{n,k}^{\text{grid}} \mathbf{S}_{k,k}^{\text{grid}} (\mathbf{V}_{p,k}^{\text{grid}})^T + (\bar{\mathbf{Z}}_p^{\text{grid}} \mathbf{1}_n^T)^T, \quad (1)$$

135 where  $\mathbf{V}_{p,k}^{\text{grid}}$  contains the first  $k$  spatial patterns,  $\mathbf{S}_{k,k}^{\text{grid}}$  is the diagonal matrix of singular values, and  $\mathbf{U}_{n,k}^{\text{grid}}$  contains the associated temporal coefficients. The vector  $\bar{\mathbf{Z}}_p^{\text{grid}}$  represents the spatial mean field,  $T$  denotes the transpose operation,  $\mathbf{1}_n$  is a vector of ones of length  $n$ .

The spatial patterns  $\mathbf{V}_{p,k}^{\text{grid}}$  form a fixed, spatially complete basis that characterizes the dominant spatial structures of the variable. These patterns are assumed to be representative of the spatial variability encountered during the interpolation period and are subsequently used to reconstruct daily fields from sparse observations.

### 3.2.2 Spatio-temporal integration through regression

140 The second step of SPR estimates the temporal amplitudes of the spatial patterns by fitting a regression model to station observations for each day of the interpolation period.

Let  $Z_d = (Z(s_1), \dots, Z(s_d))^T$  denote the vector of observed values at  $d$  gauged stations for a given day. To relate these observations to the spatial patterns, the full pattern matrix  $\mathbf{V}_{p,k}^{\text{grid}}$  is spatially restricted to the station locations, yielding the reduced matrix  $\mathbf{V}_{d,k}^{\text{grid}}$ ,  $d < p$ .

145 SPR assumes the following linear regression model:

$$Z_d - \bar{Z}_d^{\text{grid}} = \mathbf{V}_{d,k}^{\text{grid}} \beta_k + \varepsilon_d, \quad (2)$$

where  $\beta_k$  is the vector of pattern coefficients for the day considered,  $\bar{Z}_d^{\text{grid}}$  is the mean RCM field restricted to the station locations, and  $\varepsilon_d$  is a vector of residual errors.

150 This formulation is directly inspired by the PCA decomposition of the gridded fields (see Eq. (1)). It allows the spatial structure of the field to be prescribed a priori, while the temporal evolution is constrained by the available observations. In the idealized case where observations are available at all grid points, the coefficients  $\beta_k$  correspond to the PCA temporal scores. In the sparse-observation setting, they are estimated by least squares, ensuring consistency between observed values and the spatial structures imposed by the patterns.

155 The regression is performed independently for each day, yielding a sequence of coefficient vectors that capture the temporal evolution of the spatial patterns. The complete gridded field is then reconstructed using the full pattern matrix, as opposed to the restricted one in Eq. (2):

$$\hat{\mathbf{Z}}_p = \mathbf{V}_{p,k}^{\text{grid}} \hat{\beta}_k + \bar{\mathbf{Z}}_p^{\text{grid}}. \quad (3)$$



This reconstruction preserves the large-scale spatial coherence provided by the RCM-derived patterns while ensuring consistency with station observations at each time step. Rather than interpolating values directly in physical space, the method reconstructs fields as linear combinations of predefined spatial patterns, whose associated coefficients vary in time.

### 3.3 Baseline interpolation methods

Three widely used spatial interpolation methods are employed as baselines against which the performance of SPR is compared. These methods reconstruct values at ungauged locations using weighted combinations of observations from neighbouring stations and are representative of both deterministic and geostatistical approaches commonly applied in hydrology and climatology (Li and Heap, 2014; Bokke, 2017).

Inverse Distance Weighting (IDW) is a deterministic interpolation method in which observations closer to the target location receive larger weights than more distant ones (Burhanuddin et al., 2015; Margaritidis, 2024; Li and Heap, 2011, 2014; Zimmerman et al., 1999). The method assumes that spatial proximity alone governs similarity, without explicitly modeling spatial correlation or uncertainty. Despite its simplicity, IDW is frequently used as a benchmark due to its low computational cost and minimal assumptions.

Ordinary Kriging (OK) is a geostatistical method that exploits the spatial autocorrelation structure of the variable through a variogram model (Snepvangers et al., 2003). Predictions are optimal in the sense of being unbiased and of minimum variance under the assumption of second-order stationarity and isotropy. In addition to point estimates, OK provides an estimate of prediction uncertainty, which makes it a common reference method in spatial interpolation studies.

Kriging with External Drift (KED) extends OK by incorporating an auxiliary variable to represent a spatial trend in the mean structure of the field (Varentsov et al., 2020; Hengl et al., 2003). In this study, the auxiliary information corresponds to monthly climatologies derived from RCM simulations on the auxiliary period. While KED allows part of the large-scale spatial variability to be explained by the external drift, it still relies on station-based variogram modeling and assumes that residuals are stationary.

These baseline methods fundamentally differ from SPR in how spatial information is exploited. IDW, OK, and KED operate directly in the geographical space using distances and local neighbourhoods, whereas SPR relies on a low-dimensional basis of spatial patterns extracted from high-resolution gridded data. By embedding physically consistent spatial structures into the interpolation process, SPR departs from local station-centred approaches and provides a complementary framework for reconstructing spatially coherent meteorological fields.

### 3.4 Experimental design and validation framework

#### 3.4.1 Synthetic data experiments

These experiments rely on an idealized setting where a virtual station network is defined as a sub-sample of the RCM grid cells. For each of the two selected regions (see Fig. 1b), we vary two key factors — the spatial extent of the region and the density of the virtual station network — to design a set of controlled experiments. Interpolation is then performed at the remaining grid



190 cells, and the reconstructed fields are compared to the reference RCM fields, allowing a direct and controlled assessment of each method’s sensitivity to network sparsity and spatial scale.

The region size can take one of three values (large, medium, or small) corresponding to the nested rectangles shown in Fig. 1b. The network density is defined as the proportion of grid cells retained as virtual stations and is set to 10%, 30%, 50%, 70%, or 90%. For each variable, this design implies 30 distinct experiments, combining region location, spatial extent, and  
 195 network density (see Table 1).

In addition to these experiments, a stress-test experiment is designed to mimic a common practical situation in spatial interpolation: extremely sparse observation networks, as often encountered in remote regions. We focus on a large northern Quebec region (Fig. 1b) composed of 2,970 grid cells, from which only three grid cells (approximately 0.1%) are randomly selected as virtual stations.

**Table 1.** Synthetic experiments framework: For each region location (south or north), three region sizes (S, M, or L) and five network density levels (from 90% to 10%) are considered. The number of grid cells where interpolation must be performed is given by:  $(100 - \text{density}) \times$  total number of grid cells.

	Region South			Region North		
	Size L	Size M	Size S	Size L	Size M	Size S
Total # of grid cells	3025	1332	342	2970	1332	342
Network density	# of interpolated grid cells					
90%	303	133	34	297	133	34
70%	908	400	103	891	400	103
50%	1523	666	171	1485	666	171
30%	2118	932	239	2079	932	239
10%	2723	1199	308	2673	1199	308

### 200 3.4.2 Real data experiments

In these experiments, SPR is applied as intended for real-world data: station observations are provided by a real station network (see § 2.2) while RCM simulations over the auxiliary period are used to construct the spatial patterns. Interpolation is then carried out over the interpolation period, day by day and for each meteorological variable independently, at grid cells where no station observations are available.

205 We focused on a single factor: the density of the station network. Specifically, we considered only 10% and 30% densities, representing data scarcity situations and corresponding to training sets of 2 to 4 stations over a 70 000 km<sup>2</sup> region.



### 3.5 Model evaluation

For each variable, spatial interpolation is performed independently for each day, and performance metrics (see 3.5.2) are aggregated over the interpolation period. For precipitation, a  $\log(\exp(\cdot) - 1)$  transformation is applied prior to interpolation to ensure positivity after bounding values by  $10^{-5}$ . Interpolated values are then back-transformed to the original scale, and values below 0.5 mm are set to zero following Werner et al. (2019).

Since interpolation is conducted independently in time, model evaluation is formulated in the spatial domain. For synthetic experiments, virtual stations corresponding to a given network density define the training set, while the remaining grid cells form the test set. An additional validation set is obtained by randomly withholding the same proportion of grid cells from the training set, ensuring a consistent assessment of model generalization across network densities and region sizes. Validation set is used for hyperparameter selection, see 3.5.1.

For the real data experiments, a subset of stations corresponding to a given network density represent the training set while the remaining stations form the test set.

#### 3.5.1 Hyperparameter selection

Hyperparameters are selected by maximizing average performance on the validation set over the full interpolation period. Although day-specific tuning is possible, a single globally optimal configuration is retained for each method to ensure robustness and comparability across days.

For the baseline methods (IDW, OK, and KED), the tuning parameters include the IDW distance power (1–5) and the variogram model (Gaussian, Spherical, or Exponential) for OK and KED. For SPR, the number of retained spatial patterns is selected as a percentage (10%–90%) of the maximum available patterns, allowing a consistent search across regions of different sizes.

Hyperparameter selection is performed exclusively within the synthetic experiment framework, where the ground truth is fully known and systematic validation is possible across a wide range of controlled configurations. Optimizing hyperparameters under very sparse network conditions is not feasible, as it would lead to unstable estimates and potential overfitting.

Consequently, for stress-test experiments, hyperparameters are fixed to the values obtained from synthetic experiments conducted at 10% station density, which most closely matches the level of network sparsity considered in these tests. For the real station data experiments, hyperparameters are fixed to the values obtained from the synthetic experiments at the corresponding station densities (10% and 30%).

#### 3.5.2 Performance evaluation metrics

Final model performance is evaluated on the test set using the optimal hyperparameters. Interpolated values are compared to the ground truth using two complementary metrics.

The Root Mean Squared Error (RMSE) quantifies pointwise interpolation accuracy and is computed daily over the test grid cells before being averaged over the interpolation period. In addition, the Structural Similarity Index Measure (SSIM) is used



to assess the ability of each method to reproduce the spatial structure of the ground truth. SSIM values range from  $-1$  to  $1$ ,  
240 with higher values indicating greater structural similarity.

## 4 Results

### 4.1 Results of synthetic data experiments

The performance of the three baseline interpolation methods and SPR is evaluated across all synthetic experiments using daily  
RMSE and SSIM, computed over the test grid cells and averaged over the interpolation period. Results are summarized in  
245 Fig. 3 for the southern region and Fig. 4 for the northern region. In these figures, RMSE is shown on the x-axis and  $1 - \text{SSIM}$   
on the y-axis, such that points closer to the origin indicate better performance.

Across the majority of experiments and for all three meteorological variables, SPR consistently achieves the best overall  
performance, combining low interpolation errors with a strong ability to preserve structural similarity. This behavior is partic-  
ularly clear for medium and large regions in both the southern and northern domains, where SPR systematically outperforms  
250 all baseline methods.

At moderate to high station densities (50% and above), SPR dominates the comparison regardless of region size or ge-  
ographic location. At lower densities, performance differences mainly arise between SPR and KED, while OK and IDW  
consistently rank behind. In a limited number of low-density scenarios, primarily for precipitation and small regions, KED  
marginally outperforms SPR in terms of RMSE. In these cases, however, SPR generally maintains superior SSIM values,  
255 indicating a better reproduction of spatial patterns.

Overall, SPR demonstrates a favorable trade-off between pointwise accuracy and spatial coherence. Out of the 90 synthetic  
experiments considered, KED outperforms SPR in only six cases and yields comparable performance in three, while SPR  
remains superior in the vast majority of scenarios.

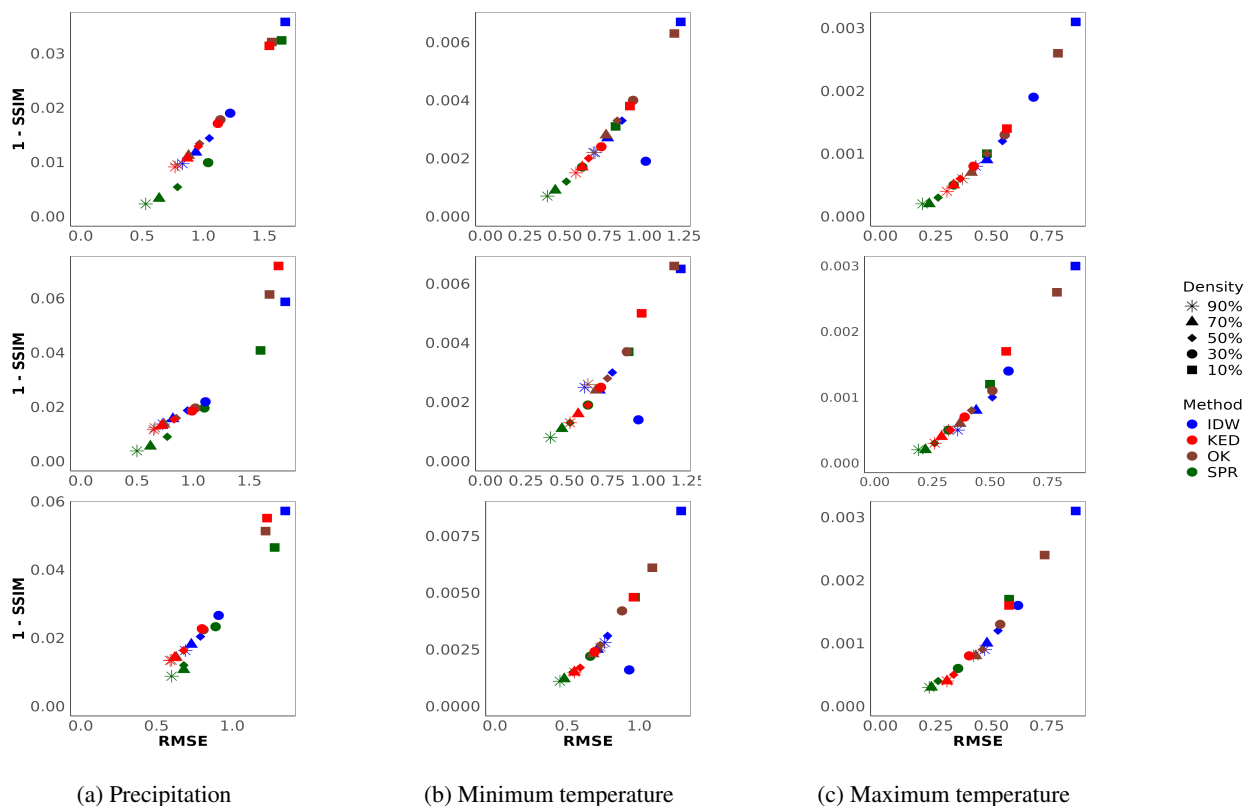


**Figure 3.** Comparison of the three baseline methods and SPR in the southern region, in terms of averaged RMSE (x-axis) and averaged 1-SSIM (y-axis). Each column represents a specific meteorological variable, while each row corresponds to a region size—ranging from the largest at the top to the smallest at the bottom. Each color represents a different interpolation method, and each plotting symbol corresponds to a specific network density. The closer a symbol is to the origin, the better the performance.

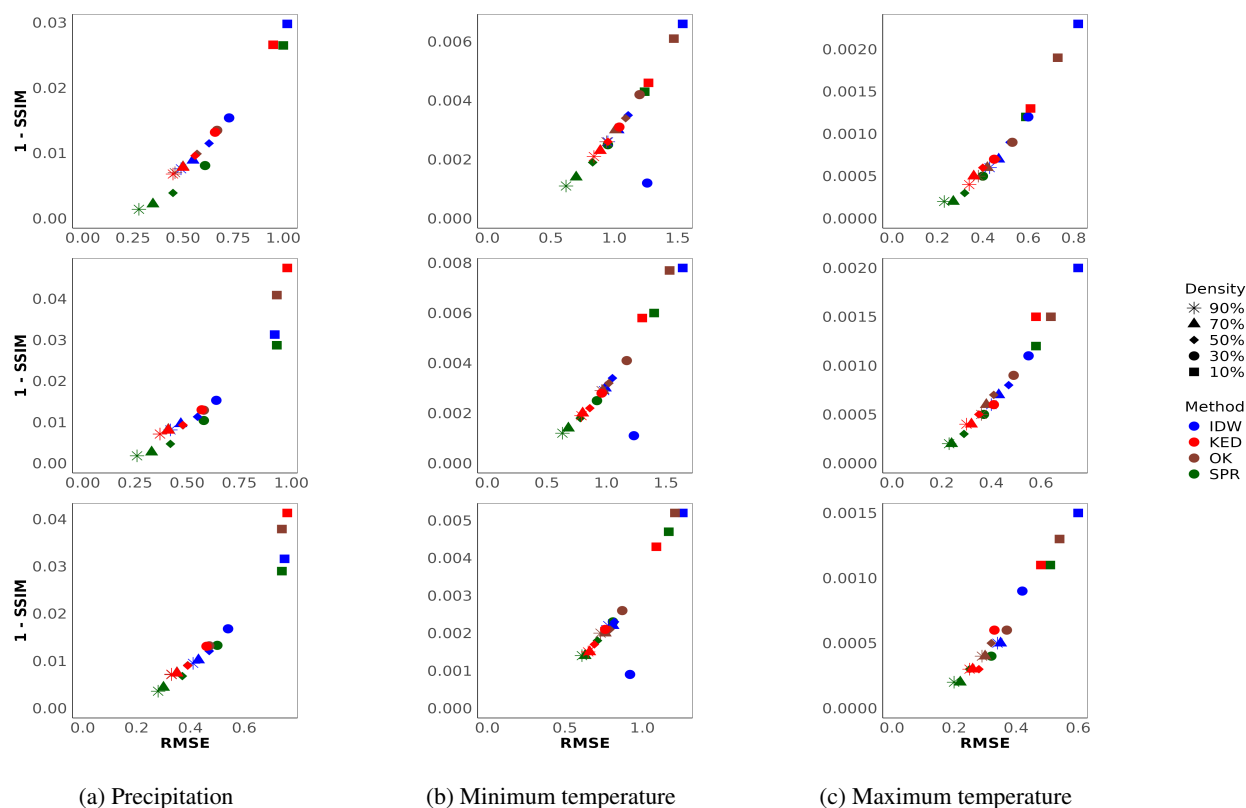


**Figure 4.** Comparison of the three baseline methods and SPR in the northern region, in terms of RMSE (x-axis) and 1-SSIM (y-axis). Each column represents a specific meteorological variable, while each row corresponds to a region size—ranging from the largest at the top to the smallest at the bottom. Each color represents a different interpolation method, and each plotting symbol corresponds to a specific network density. The closer a symbol is to the origin, the better the performance.

## 4.2 Results of synthetic stress-test experiments

260 Results (see details in Table 2) shows that SPR consistently yields lower average and lower median RMSE than KED for all three variables. For minimum and maximum temperature, SPR also achieves higher SSIM values, whereas for precipitation, KED shows a higher SSIM despite larger RMSE.

To further illustrate the differences between both methods, interpolated fields and corresponding ground truth are shown for three representative days for each variable (Fig. 5), along with the associated spatial RMSE fields (Fig. 6). KED fields are almost perfectly correlated with the climatological background (*average Spearman correlation: 0.9997*), while SPR fields exhibit weaker correlation (*0.7910*). However, SPR produces interpolated fields that are more structurally similar to the ground truth in terms of SSIM (*average SSIM: 0.4151 for SPR versus 0.2504 for KED*).

265 These results suggest that under extremely sparse observational constraints, SPR can better reproduce the spatial organization of the target fields, while KED remains strongly driven by the auxiliary climatological information used as external drift.



**Table 2.** Realistic stress-test experiments: daily RMSE statistics (mean, median, standard deviation (SD) and 2.5% and 97.5% quantiles) and average SSIM values for each variable and interpolation method. Lower RMSE and higher SSIM values indicate better performance. The best values for average and median RMSE, as well as SSIM, are shown in bold.

Variable	Method	RMSE					SSIM
		Mean	Median	SD	2.5%	97.5%	
PR	SPR	<b>3.18</b>	<b>1.97</b>	3.63	0.01	13.17	0.6654
	KED	3.39	2.16	4.06	0.04	14.02	<b>0.8044</b>
TMIN	SPR	<b>3.53</b>	<b>3.19</b>	1.8	1.08	7.79	<b>0.9636</b>
	KED	3.99	3.54	2.10	1.24	9.00	0.9541
TMAX	SPR	<b>2.59</b>	<b>2.29</b>	1.39	0.86	6.10	<b>0.9757</b>
	KED	2.97	2.59	1.61	1.01	7.09	0.9687

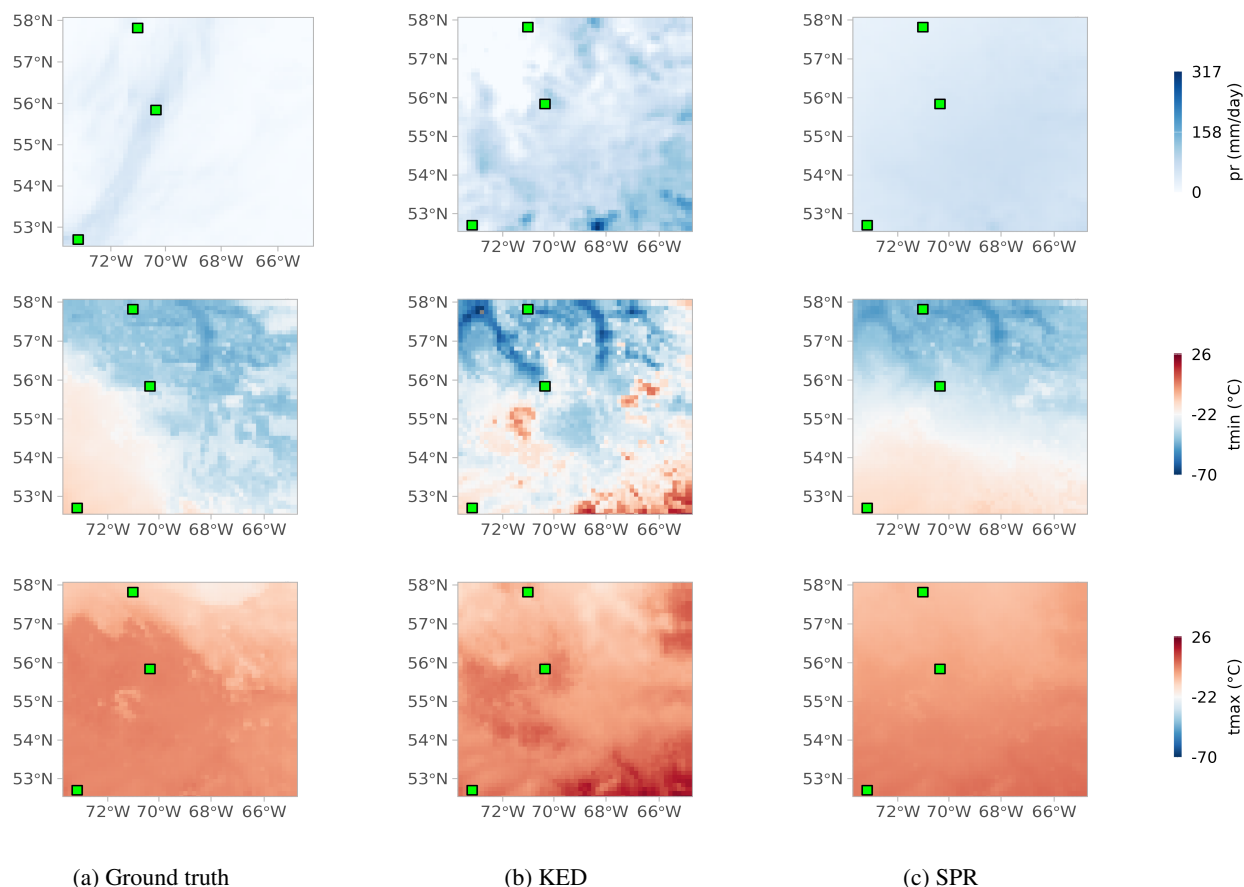


**Figure 5.** Realistic stress-test experiments: ground truth, interpolated fields of KED and SPR over the larger northern region. Green squares indicate the virtual station locations. Solid squares indicate that KED does not interpolate at virtual station locations. Rows correspond to precipitation, minimum temperature, and maximum temperature (top to bottom) on three different days.

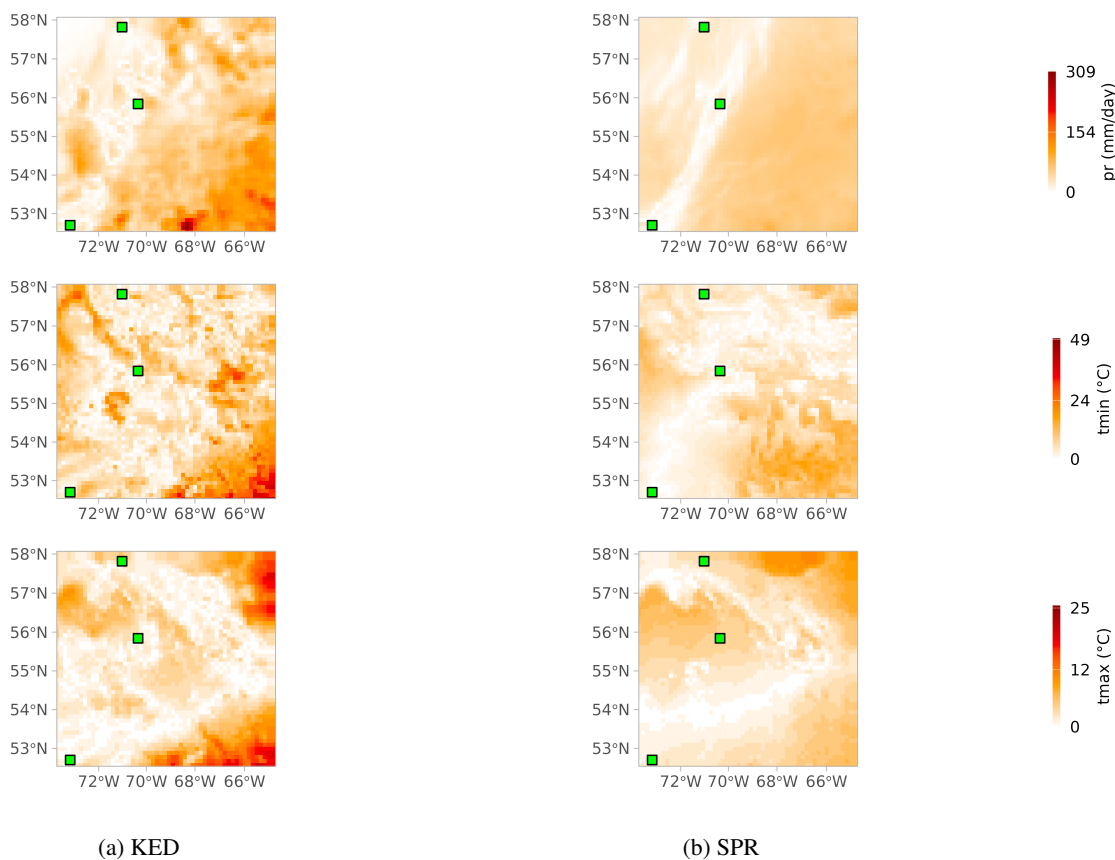


**Figure 6.** Realistic stress-test experiments: comparison of KED (right column) and SPR (left column) in the larger northern region, based on their spatial RMSE. Each row represents a specific variable: precipitation, minimum temperature and maximum temperature, from top to bottom, shown on the same three days as in Fig. 5. Green squares indicate the virtual station locations. Solid squares indicate that KED does not interpolate at virtual station locations.

### 270 4.3 Results of real data experiments

Table 3 summarizes independent validation results based on real station observations under sparse network conditions (10% and 30% densities). Overall, SPR shows strong performance across all variables when observations is very limited.

At lowest density (10%), SPR systematically achieves lower RMSE than KED for precipitation and both temperature variables, while maintaining comparable or higher SSIM values. This indicates an improved ability to reconstruct fields under very sparse networks configurations.

At 30% density, differences between SPR and KED become smaller and more variable across variables, with SPR yielding better accuracy just for maximum temperature. These results suggest that the primary advantage of SPR emerges in sparse-network settings, while its performance remains competitive as station density increases within the low-density regime considered here.



280 These findings are consistent with the synthetic experiments, which indicate that the added value of SPR is most pronounced under sparse observational coverage.

**Table 3.** Validation with real observations: daily RMSE statistics (mean, median, standard deviation (SD) and 2.5% and 97.5% quantiles) and average SSIM values for each variable and interpolation method. Lower RMSE and higher SSIM values indicate better performance. Note that 10% density correspond to 2-4 station in a region of 70.000km<sup>2</sup>

Variable	Density	Method	RMSE					SSIM
			Mean	Median	SD	2.5%	97.5%	
PR	10%	SPR	<b>2.66</b>	1.1	3.57	0.5	13.36	0.6304
		KED	3.36	1.7	4.83	0.5	15.35	<b>0.6309</b>
	30%	SPR	2.73	1.09	4.02	0.5	13.42	0.6645
		KED	<b>2.51</b>	0.99	3.51	0.5	12.31	<b>0.6784</b>
TMIN	10%	SPR	<b>2.39</b>	2.20	0.89	1.09	4.66	<b>0.9517</b>
		KED	3.65	3.25	1.63	1.52	7.65	0.9406
	30%	SPR	2.34	2.18	0.78	1.22	4.22	0.8995
		KED	<b>2.21</b>	2.08	0.78	0.97	4.06	<b>0.9202</b>
TMAX	10%	SPR	<b>1.81</b>	1.56	0.90	0.86	4.17	<b>0.9875</b>
		KED	1.84	1.53	1.02	0.83	4.63	0.9865
	30%	SPR	1.33	1.18	0.53	0.69	2.82	0.9935
		KED	<b>1.32</b>	1.16	0.59	0.70	2.96	<b>0.9936</b>

#### 4.4 Sensitivity analysis of SPR performance

A factor-wise sensitivity analysis of SPR is conducted using synthetic experiments to assess the influence of station network density, region size, and region location across the three meteorological variables. The main conclusions are summarized below, while detailed results are not shown.

Station network density is the dominant factor controlling SPR performance: increasing density systematically reduces RMSE and uncertainty in both regions. Precipitation exhibits higher RMSE and larger uncertainty than temperature variables, reflecting its greater interpolation difficulty.

In contrast, region size has a limited impact on average performance, with RMSE remaining broadly stable across scales. Region location affects performance in a variable-dependent manner: precipitation errors are lower in the north, whereas temperature errors are higher, suggesting that differences in spatial structure affect interpolation accuracy.

## 5 Discussion and conclusions

In this work, we introduced Spatial Pattern Regression (SPR), a statistical framework for generating meteorological data that explicitly leverages the spatial structures embedded in RCM simulations. SPR formulates spatial interpolation as a low-rank



295 reconstruction problem, in which daily meteorological fields are represented as linear combinations of spatial patterns extracted  
from auxiliary gridded data through SVD/PCA. Overall, SPR reframes interpolation by prioritizing physically consistent spatial  
organization rather than purely local spatial proximity.

More specifically, the proposed method addresses a key limitation of existing interpolation approaches, which typically  
incorporate auxiliary information — such as elevation or RCM-based climatologies — through predefined covariates or drift  
300 terms, thereby failing to fully leverage the rich spatial structures embedded in gridded datasets. By explicitly extracting spatial  
patterns from RCM covariance structures, SPR provides a principled mechanism for integrating physically consistent spatial  
organization into interpolation, without directly constraining interpolated values toward the auxiliary information. Instead,  
the auxiliary dataset serves to define the dominant modes of spatial variability rather than to impose absolute values. This  
conceptual shift — from using auxiliary information to constrain absolute values toward using it to define spatial organization  
305 — underpins the development of the proposed methodology and allows SPR to accommodate a wide range of auxiliary gridded  
products, including RCM outputs, elevation fields, radar products, or remote sensing data.

The experimental results demonstrate that SPR provides accurate and robust interpolations across a wide range of config-  
urations. SPR performs competitively with established baseline methods, including KED, OK, and IDW, and shows a clear  
advantage under very sparse station network conditions. Among the baseline approaches, KED remains the strongest compar-  
310 ator, consistent with previous findings in spatial interpolation studies (Bishop and McBratney, 2001). Our results also confirm  
that station density and region location are first-order drivers of interpolation uncertainty, in agreement with earlier work  
(Stahl et al., 2006; Li and Heap, 2014; Wagner et al., 2012). Importantly, SPR does not uniformly outperform KED across all  
configurations, but its relative benefit becomes most apparent when observational information is severely limited.

A key contribution of SPR lies in its ability to ensure spatial consistency between interpolated historical fields and fu-  
315 ture climate simulations. In climate change impact studies, interpolated meteorological data are commonly used to calibrate  
hydrological models over historical periods, while RCM simulations are employed to assess future changes. By reproducing  
spatial structures derived from RCM simulations in the interpolated fields, SPR helps reduce structural inconsistencies between  
calibration and projection phases. This property is particularly relevant for distributed hydrological modeling, where spatial  
coherence strongly influences simulated fluxes and states.

320 The extraction of spatial patterns relies on the representativeness of the auxiliary period, which must adequately capture the  
dominant spatial variability and characteristic meteorological structures of the target variable. Beyond this requirement, the  
auxiliary period can be selected flexibly and does not need to overlap temporally with the observation period. This flexibility  
distinguishes SPR from reanalysis-based approaches, which rely on complex data assimilation systems and strict temporal  
alignment between observations and model states (Gasset et al., 2021). SPR is not intended to replace reanalysis products, but  
325 rather to provide a lightweight and transparent alternative when dense observational networks or full assimilation frameworks  
are unavailable.

Several limitations and avenues for improvement remain. In its current form, SPR relies on a fixed number of leading spatial  
patterns. Allowing the adaptive selection of spatial patterns, potentially including lower-ranked modes that capture event-  
specific features, may further enhance performance. In addition, the present implementation estimates regression coefficients



330 independently for each day, ignoring temporal dependence. Incorporating temporal regularization or joint spatio-temporal modeling of the coefficients represents a natural extension of the framework.

In conclusion, SPR offers an efficient and conceptually coherent alternative for spatial interpolation of meteorological variables, particularly suited to poorly instrumented regions where station density is low and spatial consistency is critical. The current formulation provides a solid baseline for future developments aimed at integrating temporal dependence, nonlinearity, and additional sources of spatial information, with clear potential for operational hydrological and climate impact applications.

*Code and data availability.* All analyses were performed using the R programming language version 4.4.3. The analysis scripts developed for this study are not publicly archived but can be provided by the corresponding author upon reasonable request. The primary data source consists of daily climate simulations from the ClimEx project (<https://climex-data.srv.lrz.de/Public/>). We used one ensemble member (kcj) from the CanESM2-driven simulations. Real station observations were obtained from the national monitoring network operated by Environment and Climate Change Canada (ECCC). Data were downloaded automatically through the official bulk data API ([https://climate.weather.gc.ca/climate\\_data/bulk\\_data\\_e.html](https://climate.weather.gc.ca/climate_data/bulk_data_e.html)).

*Author contributions.* **Vihotogbé Houssou:** Conceptualization, Methodology, Software, Validation, Formal analysis, Data curation, Visualization, Writing - original draft, Writing - review & editing. **Julie Carreau:** Conceptualization, Methodology, Supervision, Resources, Funding acquisition, Validation, Writing - review & editing.

345 *Competing interests.* The authors declare that they have no conflict of interest.

*Acknowledgements.* The authors would like to acknowledge funding by the Natural Sciences and Engineering Research Council of Canada (NSERC), by Fonds de Recherche du Québec Nature et Technologies (FRQNT) and by IVADO.



## References

- Abémgnigni Njifon, M., and Schuhmacher, D.: Graph convolutional networks for spatial interpolation of correlated data, *Spat. Stat.*, 60, 100822, [<https://doi.org/10.1016/j.spasta.2024.100822>](<https://doi.org/10.1016/j.spasta.2024.100822>), 2024.
- Amato, F., Guignard, F., Robert, S., and Kanevski, M.: A novel framework for spatio-temporal prediction of environmental data using deep learning, *Sci. Rep.*, 10, 22243, [<https://doi.org/10.1038/s41598-020-79148-7>](<https://doi.org/10.1038/s41598-020-79148-7>), 2020.
- Baxevani, A., and Lennartsson, J.: A spatiotemporal precipitation generator based on a censored latent Gaussian field, *Water Resour. Res.*, 51, 4338–4358, [<https://doi.org/10.1002/2014WR016455>](<https://doi.org/10.1002/2014WR016455>), 2015.
- 355 Benoit, L., Allard, D., and Mariethoz, G.: Stochastic Rainfall Modeling at Sub-kilometer Scale, *Water Resour. Res.*, 54, 4108–4130, [<https://doi.org/10.1029/2018WR022817>](<https://doi.org/10.1029/2018WR022817>), 2018.
- Bishop, T. F. A., and McBratney, A. B.: A comparison of prediction methods for the creation of field-extent soil property maps, *Geoderma*, 103, 149–160, [[https://doi.org/10.1016/S0016-7061\(01\)00074-X](https://doi.org/10.1016/S0016-7061(01)00074-X)]([https://doi.org/10.1016/S0016-7061\(01\)00074-X](https://doi.org/10.1016/S0016-7061(01)00074-X)), 2001.
- Bokke, A.: Comparative Evaluation of Spatial Interpolation Methods for Estimation of Missing Meteorological Variables over Ethiopia, *J. Water Resour. Prot.*, 9, 945–959, [<https://doi.org/10.4236/jwarp.2017.98063>](<https://doi.org/10.4236/jwarp.2017.98063>), 2017.
- 360 Burhanuddin, S. N. Z. A., Deni, S., and Mohamed Ramli, N.: Geometric median for missing rainfall data imputation, *AIP Conf. Proc.*, 1643, 113–119, [<https://doi.org/10.1063/1.4907433>](<https://doi.org/10.1063/1.4907433>), 2015.
- Burrough, P., and McDonnell, R.: *Principles of Geographic Information Systems*, Oxford Univ. Press, Oxford, 1998.
- Caldera, H. P. G. M., Piyathisse, V., and Nandalal, K. D. W.: A Comparison of Methods of Estimating Missing Daily Rainfall Data, *Engineer (Sri Lanka)*, 49, 1, [<https://doi.org/10.4038/engineer.v49i4.7232>](<https://doi.org/10.4038/engineer.v49i4.7232>), 2016.
- 365 Carreau, J., and Guinot, V.: A PCA spatial pattern based artificial neural network downscaling model for urban flood hazard assessment, *Adv. Water Resour.*, 147, 103821, [<https://doi.org/10.1016/j.advwatres.2020.103821>](<https://doi.org/10.1016/j.advwatres.2020.103821>), 2021.
- Cattiaux, J., Vautard, R., Cassou, C., Yiou, P., Masson-Delmotte, V., and Codron, F.: Winter 2010 in Europe: a cold extreme in a warming climate, *Geophys. Res. Lett.*, 37, L20704, [<https://doi.org/10.1029/2010GL044613>](<https://doi.org/10.1029/2010GL044613>), 2010.
- 370 Chen, J., Brissette, F. P., Liu, P., and Xia, J.: Using raw regional climate model outputs for quantifying climate change impacts on hydrology, *Hydrol. Process.*, 31, 4398–4413, [<https://doi.org/10.1002/hyp.11368>](<https://doi.org/10.1002/hyp.11368>), 2017.
- Cheng, G., and Lu, L.: Comparison of spatial interpolation methods, *Adv. Earth Sci.*, 15, 260–265, 2000.
- Danabasoglu, G., Lamarque, J.-F., Bacmeister, J., Bailey, D. A., DuVivier, A. K., Edwards, J., Emmons, L. K., Fasullo, J., Garcia, R., Gettelman, A., Hannay, C., Holland, M. M., Large, W. G., Lauritzen, P. H., Lawrence, D. M., Lenaerts, J. T. M., Lindsay, K., Lipscomb, W. H., Mills, M. J., Neale, R., Oleson, K. W., Otto-Bliesner, B., Phillips, A. S., Sacks, W., Tilmes, S., van Kampenhout, L., Vertenstein, M., Bertini, A., Dennis, J., Deser, C., Fischer, C., Fox-Kemper, B., Kay, J. E., Kinnison, D., Kushner, P. J., Larson, V. E., Long, M. C., Mickelson, S., Moore, J. K., Nienhouse, E., Polvani, L., Rasch, P. J., and Strand, W. G.: The Community Earth System Model Version 2 (CESM2), *J. Adv. Model. Earth Syst.*, 12, e2019MS001916, [<https://doi.org/10.1029/2019MS001916>](<https://doi.org/10.1029/2019MS001916>), 2020.
- 375 Doersch, C.: Tutorial on variational autoencoders, arXiv preprint, arXiv:1606.05908, 2016.
- Eklundh, L., and Pilesjö, P.: Regionalization and spatial estimation of Ethiopian mean annual rainfall, *Int. J. Climatol.*, 10, 473–494, [<https://doi.org/10.1002/joc.3370100505>](<https://doi.org/10.1002/joc.3370100505>), 1990.
- Faghih, M., and Brissette, F.: Temporal and Spatial Amplification of Extreme Rainfall and Extreme Floods in a Warmer Climate, *J. Hydrometeorol.*, 24, 1331–1347, [<https://doi.org/10.1175/JHM-D-22-0224.1>](<https://doi.org/10.1175/JHM-D-22-0224.1>), 2023.



- 385 Falola, Y., Churilova, P., Liu, R., Huang, C.-K., Delgado, J. F., and Misra, S.: Generating extremely low-dimensional representation of subsurface earth models using vector quantization and deep Autoencoder, *Petrol. Res.*, 2024, [<https://doi.org/10.1016/j.ptlrs.2024.07.001>] (<https://doi.org/10.1016/j.ptlrs.2024.07.001>), 2024.
- Flato, G. M.: Earth system models: an overview, *WIREs Clim. Change*, 2, 783–800, [<https://doi.org/10.1002/wcc.148>](<https://doi.org/10.1002/wcc.148>), 2011.
- 390 Fletcher, C. G., McNally, W., Virgin, J. G., and King, F.: Toward Efficient Calibration of Higher-Resolution Earth System Models, *J. Adv. Model. Earth Syst.*, 14, e2021MS002836, [<https://doi.org/10.1029/2021MS002836>](<https://doi.org/10.1029/2021MS002836>), 2022.
- Gasset, N., Fortin, V., Dimitrijevic, M., Carrera, M., Bilodeau, B., Muncaster, R., Gaborit, É., Roy, G., Pentcheva, N., Bulat, M., Wang, X., Pavlovic, R., Lespinas, F., Khedhaouiria, D., and Mai, J.: A 10 km North American precipitation and land-surface reanalysis based on the GEM atmospheric model, *Hydrol. Earth Syst. Sci.*, 25, 4917–4945, [<https://doi.org/10.5194/hess-25-4917-2021>](<https://doi.org/10.5194/hess-25-4917-2021>), 2021.
- 395 Hartkamp, A. D., de Beurs, K., Stein, A., and White, J.: Interpolation Techniques for Climate Variables, GIS Series 99-01, CIMMYT, Mexico, 1999.
- Hasanpour Kashani, M., and Dinpashoh, Y.: Evaluation of efficiency of different estimation methods for missing climatological data, *Stoch. Environ. Res. Risk Assess.*, 26, 59–71, [<https://doi.org/10.1007/s00477-011-0536-y>](<https://doi.org/10.1007/s00477-011-0536-y>), 2012.
- 400 Hengl, T.: A Practical Guide to Geostatistical Mapping of Environmental Variables, *Geoderma*, 140, 417–427, 2007.
- Hengl, T., Heuvelink, G. B. M., and Stein, A.: Comparison of kriging with external drift and regression-kriging, *Tech. Note*, 2003.
- Hijmans, R. J., Cameron, S. E., Parra, J. L., Jones, P. G., and Jarvis, A.: Very high resolution interpolated climate surfaces for global land areas, *Int. J. Climatol.*, 25, 1965–1978, [<https://doi.org/10.1002/joc.1276>](<https://doi.org/10.1002/joc.1276>), 2005.
- Hutchinson, M. F.: Interpolating mean rainfall using thin plate smoothing splines, *Int. J. Geogr. Inf. Syst.*, 9, 385–403, [<https://doi.org/10.1080/02693799508902045>](<https://doi.org/10.1080/02693799508902045>), 1995.
- 405 Hutchinson, M. F., McKenney, D. W., Lawrence, K., Pedlar, J. H., Hopkinson, R. F., Milewska, E., and Papadopol, P.: Development and Testing of Canada-Wide Interpolated Spatial Models of Daily Minimum–Maximum Temperature and Precipitation for 1961–2003, *J. Appl. Meteorol. Climatol.*, 48, 725–741, [<https://doi.org/10.1175/2008JAMC1979.1>](<https://doi.org/10.1175/2008JAMC1979.1>), 2009.
- Hwang, Y., Clark, M., Rajagopalan, B., and Leavesley, G.: Spatial interpolation schemes of daily precipitation for hydrologic modeling, *Stoch. Environ. Res. Risk Assess.*, 26, 295–320, [<https://doi.org/10.1007/s00477-011-0509-1>](<https://doi.org/10.1007/s00477-011-0509-1>), 2012.
- IPCC: Annex VII: Glossary, in: *Climate Change 2021: The Physical Science Basis*, Cambridge Univ. Press, Cambridge and New York, 2215–2256, [<https://doi.org/10.1017/9781009157896.022>](<https://doi.org/10.1017/9781009157896.022>), 2021.
- Lam, N.: Spatial Interpolation Methods: A Review, *Cartogr. Geogr. Inf. Sci.*, 10, 129–150, [<https://doi.org/10.1559/152304083783914958>] (<https://doi.org/10.1559/152304083783914958>), 1983.
- 415 Lauer, A., Pausata, F. S. R., Leroyer, S., and Argueso, D.: Effect of urban heat island mitigation strategies on precipitation and temperature in Montreal, Canada: Case studies, *PLOS Clim.*, 2, e0000196, [<https://doi.org/10.1371/journal.pclm.0000196>](<https://doi.org/10.1371/journal.pclm.0000196>), 2023.
- Leduc, M., Mailhot, A., Frigon, A., and others: The ClimEx Project: A 50-Member Ensemble of Climate Change Projections at 12-km Resolution over Europe and Northeastern North America with the Canadian Regional Climate Model (CRCM5), *J. Appl. Meteorol. Climatol.*, 58, 663–693, [<https://doi.org/10.1175/JAMC-D-18-0021.1>](<https://doi.org/10.1175/JAMC-D-18-0021.1>), 2019.
- 420



- Li, J., and Heap, A. D.: A review of spatial interpolation methods for environmental scientists, *Geoscience Australia*, ISBN 9781921498305, 2008.
- Li, J., and Heap, A. D.: A review of comparative studies of spatial interpolation methods in environmental sciences: Performance and impact factors, *Ecol. Inform.*, 6, 228–241, [<https://doi.org/10.1016/j.ecoinf.2010.12.003>](<https://doi.org/10.1016/j.ecoinf.2010.12.003>), 2011.
- 425 Li, J., and Heap, A. D.: Spatial interpolation methods applied in the environmental sciences: A review, *Environ. Model. Softw.*, 53, 173–189, [<https://doi.org/10.1016/j.envsoft.2013.12.008>](<https://doi.org/10.1016/j.envsoft.2013.12.008>), 2014.
- Li, Y.: Review on spatial interpolation methods of temperature data from meteorological stations, *Prog. Geogr.*, 2014.
- Link, R., Snyder, A., Lynch, C., Hartin, C., Kravitz, B., and Bond-Lamberty, B.: Fldgen v1.0: an emulator with internal variability and space–time correlation for Earth system models, *Geosci. Model Dev.*, 12, 1477–1489, [<https://doi.org/10.5194/gmd-12-1477-2019>](<https://doi.org/10.5194/gmd-12-1477-2019>), 2019.
- 430 Livneh, B., Bohn, T. J., Pierce, D. W., Munoz-Arriola, F., Nijssen, B., Vose, R., Cayan, D. R., and Brekke, L.: A spatially comprehensive, hydrometeorological data set for Mexico, the U.S., and Southern Canada 1950–2013, *Sci. Data*, 2, 150042, [<https://doi.org/10.1038/sdata.2015.42>](<https://doi.org/10.1038/sdata.2015.42>), 2015.
- 435 Looper, J. P., and Vieux, B. E.: An assessment of distributed flash flood forecasting accuracy using radar and rain gauge input for a physics-based distributed hydrologic model, *J. Hydrol.*, 412–413, 114–132, [<https://doi.org/10.1016/j.jhydrol.2011.05.046>](<https://doi.org/10.1016/j.jhydrol.2011.05.046>), 2012.
- Lucas-Picher, P., Riboust, P., Somot, S., and Laprise, R.: Reconstruction of the Spring 2011 Richelieu River Flood by Two Regional Climate Models and a Hydrological Model, *J. Hydrometeorol.*, 16, 36–54, [<https://doi.org/10.1175/JHM-D-14-0116.1>](<https://doi.org/10.1175/JHM-D-14-0116.1>), 2015.
- 440 Lucas-Picher, P., Arsenault, R., Poulin, A., Ricard, S., Lachance-Cloutier, S., and Turcotte, R.: Application of a High-Resolution Distributed Hydrological Model on a U.S.–Canada Transboundary Basin: Simulation of the Multiyear Mean Annual Hydrograph and 2011 Flood of the Richelieu River Basin, *J. Adv. Model. Earth Syst.*, 12, e2019MS001709, [<https://doi.org/10.1029/2019MS001709>](<https://doi.org/10.1029/2019MS001709>), 2020.
- 445 Ly, S., Charles, C., and Degré, A.: Different methods for spatial interpolation of rainfall data for operational hydrology and hydrological modeling at watershed scale: A review, *Biotechnol. Agron. Soc. Environ.*, 17, 392–406, [<https://popups.uliege.be/1780-4507/index.php?id=10003>](<https://popups.uliege.be/1780-4507/index.php?id=10003>), 2013.
- Maduako, I., Ebinne, E., Idorenyin, U., and Ndukwu, R.: Accuracy Assessment and Comparative Analysis of IDW, Spline and Kriging in Spatial Interpolation of Landform (Topography): An Experimental Study, *J. Geogr. Inf. Syst.*, 9, 354–371, [<https://doi.org/10.4236/jgis.2017.93022>](<https://doi.org/10.4236/jgis.2017.93022>), 2017.
- 450 Margaritidis, A.: Comparison of Spatial Interpolation Methods of Precipitation Data in Central Macedonia, Greece, *Comput. Water Energy Environ. Eng.*, 13, 13–37, [<https://doi.org/10.4236/cweee.2024.131002>](<https://doi.org/10.4236/cweee.2024.131002>), 2024.
- Mirbod, M., Rajabzadeh Ghatari, A., Saati, S., and Shoar, M.: Industrial parts change recognition model using machine vision, image processing in the framework of industrial information integration, *J. Ind. Inf. Integr.*, 26, 100277, [<https://doi.org/10.1016/j.jii.2021.100277>](<https://doi.org/10.1016/j.jii.2021.100277>)(<https://doi.org/10.1016/j.jii.2021.100277>), 2022.
- 455 Mitas, L., and Mitasova, H.: Spatial interpolation, in: *Geographical Information Systems: Principles, Techniques, Management and Applications*, Wiley, Hoboken, 1999.
- Monahan, A. H., Fyfe, J. C., Ambaum, M. H. P., Stephenson, D. B., and North, G. R.: Empirical Orthogonal Functions: The Medium is the Message, *J. Clim.*, 22, 6501–6514, [<https://doi.org/10.1175/2009JCLI3062.1>](<https://doi.org/10.1175/2009JCLI3062.1>), 2009.



- 460 Muñoz-Sabater, J., Dutra, E., Agustí-Panareda, A., Albergel, C., Arduini, G., Balsamo, G., Boussetta, S., Choulga, M., Harrigan, S., Hersbach, H., Martens, B., Miralles, D. G., Piles, M., Rodríguez-Fernández, N. J., Zsoter, E., Buontempo, C., and Thépaut, J.-N.: ERA5-Land: a state-of-the-art global reanalysis dataset for land applications, *Earth Syst. Sci. Data*, 13, 4349–4383, [<https://doi.org/10.5194/essd-13-4349-2021>](<https://doi.org/10.5194/essd-13-4349-2021>), 2021.
- Pavão, C., França, G., Marotta, G., Mnezes, P. H. B., Neto, G., and Roig, H.: Spatial Interpolation Applied to Crustal Thickness in Brazil, *J. Geogr. Inf. Syst.*, 4, 142–152, 2012.
- 465 Prinn, R. G.: Development and application of earth system models, *Proc. Natl. Acad. Sci. USA*, 110, suppl. 1, 3673–3680, [<https://doi.org/10.1073/pnas.1107470109>](<https://doi.org/10.1073/pnas.1107470109>), 2013.
- R Core Team: R: A Language and Environment for Statistical Computing, R Foundation for Statistical Computing, Vienna, Austria, [<https://www.R-project.org/>](<https://www.R-project.org/>), 2023.
- 470 Razafimaharo, C., Krähenmann, S., Höpp, S., Rauthe, M., and Deutschländer, T.: New high-resolution gridded dataset of daily mean, minimum, and maximum temperature and relative humidity for Central Europe (HYRAS), *Theor. Appl. Climatol.*, 142, 1531–1553, [<https://doi.org/10.1007/s00704-020-03388-w>](<https://doi.org/10.1007/s00704-020-03388-w>), 2020.
- Segond, M.-L., Wheeler, H. S., and Onof, C.: The significance of spatial rainfall representation for flood runoff estimation: A numerical evaluation based on the Lee catchment, UK, *J. Hydrol.*, 347, 116–131, [<https://doi.org/10.1016/j.jhydrol.2007.09.040>](<https://doi.org/10.1016/j.jhydrol.2007.09.040>), 2007.
- 475 Snepvangers, J. J. J. C., Heuvelink, G. B. M., and Huisman, J. A.: Soil water content interpolation using spatio-temporal kriging with external drift, *Geoderma*, 112, 253–271, [[https://doi.org/10.1016/S0016-7061\(02\)00310-5](https://doi.org/10.1016/S0016-7061(02)00310-5)]([https://doi.org/10.1016/S0016-7061\(02\)00310-5](https://doi.org/10.1016/S0016-7061(02)00310-5)), 2003.
- Sokolchuk, K., and Sokac, M.: Comparison of spatial interpolation methods of hydrological data on example of the Pripyat river basin (within Ukraine), *Acta Hydrol. Slovaca*, 2022.
- 480 Stahl, K., Moore, R. D., Floyer, J. A., Asplin, M. G., and McKendry, I. G.: Comparison of approaches for spatial interpolation of daily air temperature in a large region with complex topography and highly variable station density, *Agric. For. Meteorol.*, 139, 224–236, [<https://doi.org/10.1016/j.agrformet.2006.07.004>](<https://doi.org/10.1016/j.agrformet.2006.07.004>), 2006.
- Tan, Q., and Xu, X.: Comparative Analysis of Spatial Interpolation Methods: an Experimental Study, *Sens. Transducers*, 165, 155–163, 2014.
- 485 Tang, G., Clark, M. P., Newman, A. J., Wood, A. W., Papalexiou, S. M., Vionnet, V., and Whitfield, P. H.: SCDNA: a serially complete precipitation and temperature dataset for North America from 1979 to 2018, *Earth Syst. Sci. Data*, 12, 2381–2409, [<https://doi.org/10.5194/essd-12-2381-2020>](<https://doi.org/10.5194/essd-12-2381-2020>), 2020.
- Taylor, M. H., Losch, M., Wenzel, M., and Schröter, J.: On the Sensitivity of Field Reconstruction and Prediction Using Empirical Orthogonal Functions Derived from Gappy Data, *J. Clim.*, 26, 9194–9205, [<https://doi.org/10.1175/JCLI-D-13-00089.1>](<https://doi.org/10.1175/JCLI-D-13-00089.1>), 2013.
- 490 JCLI-D-13-00089.1), 2013.
- Varentsov, M., Esau, I., and Wolf, T.: High-resolution temperature mapping by geostatistical kriging with external drift from large-eddy simulations, *Mon. Weather Rev.*, 148, 1029–1048, [<https://doi.org/10.1175/MWR-D-19-0196.1>](<https://doi.org/10.1175/MWR-D-19-0196.1>), 2020.
- Verworn, A., and Haberlandt, U.: Spatial interpolation of hourly rainfall – effect of additional information, variogram inference and storm properties, *Hydrol. Earth Syst. Sci.*, 15, 569–584, [<https://doi.org/10.5194/hess-15-569-2011>](<https://doi.org/10.5194/hess-15-569-2011>), 2011.



- Wagner, P. D., Fiener, P., Wilken, F., Kumar, S., and Schneider, K.: Comparison and evaluation of spatial interpolation schemes for daily rainfall in data scarce regions, *J. Hydrol.*, 464–465, 388–400, [<https://doi.org/10.1016/j.jhydrol.2012.07.026>](<https://doi.org/10.1016/j.jhydrol.2012.07.026>), 2012.
- 500 Wang, Z., Bovik, A. C., Sheikh, H. R., and Simoncelli, E. P.: Image quality assessment: from error visibility to structural similarity, *IEEE Trans. Image Process.*, 13, 600–612, [<https://doi.org/10.1109/TIP.2003.819861>](<https://doi.org/10.1109/TIP.2003.819861>), 2004.
- Wang, W., Yin, S., Yu, B., and Wang, S.: CLIGEN parameter regionalization for mainland China, *Earth Syst. Sci. Data*, 13, 2945–2962, [<https://doi.org/10.5194/essd-13-2945-2021>](<https://doi.org/10.5194/essd-13-2945-2021>), 2021.
- Warren, F., and others: Canada in a Changing Climate: Regional Perspectives Report, Government of Canada, Ottawa, ON, [<https://changingclimate.ca/regional-perspectives/>](<https://changingclimate.ca/regional-perspectives/>), 2022.
- 505 Werner, A. T., Schnorbus, M. A., Shrestha, R. R., Cannon, A. J., Zwiers, F. W., Dayon, G., and Anslow, F.: A long-term, temporally consistent, gridded daily meteorological dataset for northwestern North America, *Sci. Data*, 6, 1–16, [<https://doi.org/10.1038/sdata.2018.299>](<https://doi.org/10.1038/sdata.2018.299>), 2019.
- Zhang, T., Zhou, Y., Zhao, K., Zhu, Z., Chen, G., Hu, J., and Wang, L.: A global dataset of daily maximum and minimum near-surface air temperature at 1 km resolution over land (2003–2020), *Earth Syst. Sci. Data*, 14, 5637–5649, [<https://doi.org/10.5194/essd-14-5637-2022>](<https://doi.org/10.5194/essd-14-5637-2022>), 2022.
- 510 Zimmerman, D., Pavlik, C., Ruggles, A., and Armstrong, M. P.: An Experimental Comparison of Ordinary and Universal Kriging and Inverse Distance Weighting, *Math. Geol.*, 31, 375–390, [<https://doi.org/10.1023/A:1007586507433>](<https://doi.org/10.1023/A:1007586507433>), 1999.